Ion acoustic turbulence in a 100-A LaB_6 hollow cathode

Benjamin A. Jorns,* Ioannis G. Mikellides, and Dan M. Goebel
Electric Propulsion Group, Jet Propulsion Laboratory, California Institute of Technology, Pasadena, California 91109, USA
(Received 10 September 2014; published 5 December 2014)

The temporal fluctuations in the near plume of a 100-A LaB_6 hollow cathode are experimentally investigated. A probe array is employed to measure the amplitude and dispersion of axial modes in the plume, and these properties are examined parametrically as a function of cathode operating conditions. The onset of ion acoustic turbulence is observed at high current and is characterized by a power spectrum that exhibits a cutoff at low frequency and an inverse dependence on frequency at high values. The amplitude of the turbulence is found to decrease with flow rate but to depend nonmonotonically on discharge current. Estimates of the anomalous collision frequency based on experimental measurements indicate that the ion acoustic turbulence collision frequency can exceed the classical rate at high discharge current densities by nearly two orders of magnitude.

DOI: 10.1103/PhysRevE.90.063106 PACS number(s): 52.35.Fp, 52.35.Ra, 52.75.Di

I. INTRODUCTION

Despite the fact that the hollow cathode is a staple component of many of the electric propulsion systems flown today, there are two major physical mechanisms governing the behavior of these flight-critical elements that remain unclear. The first is the presence of anomalous resistivity in the cathode plume [1]. Without an understanding of this effect, simulations of hollow cathodes must be informed by experimental measurements. This dependence limits the ability of models to examine new design iterations and curtails their predictive capability for long life behavior. The second anomalous effect is the production of ions in the cathode plume with energy significantly in excess of the discharge voltage. These high energy ions have been shown to be capable of completely eroding away the cathode keeper face [2,3]—a result which typically results in component failure.

To date, our lack of understanding of the cathode physical processes has not prevented the successful qualification of deep-space missions that rely on this technology [4–7]; however, in light of new NASA programs that are calling for higher power EP missions with extended lifetimes, it is becoming increasingly important to resolve the hollow cathode unknowns. Indeed, the only extended lifetime study of a high-current hollow cathode ever performed demonstrated a maximum lifetime of just 8000 h at 100 A [8]. In light of this failing, the need is apparent to design cathodes with improved capability, and a more complete understanding of the anomalous processes governing cathode behavior can help facilitate this effort.

While most investigations of hollow cathodes have focused on the problem of high energy ion formation [9–17], the importance of anomalous resistivity to cathode operation has only recently come to light. In particular, while attempting to simulate the partially ionized gas in a 1.5-cm-diameter, 25-A discharge hollow cathode used in the Nuclear Electric Xenon Ion System (NEXIS), Mikellides *et al.* found that classical resistivity alone was insufficient to explain the gradients of plasma potential and electron temperature measured in the orifice and near plume of the device [1,18]. The same conclusions were reached after numerical simulations were performed of a smaller cathode (0.635 cm, 13 A) used in the NASA Solar Electric Propulsion Technology Applications Readiness (NSTAR) engine [16]. In an effort to provide a physical explanation as to why anomalous collisions should exist in these devices, Mikellides *et al.* showed that the electron Mach number and electron to ion temperature ratio were high enough in the orifice and near-plume plasma to onset ion acoustic turbulence (IAT)—a mode commonly found in current-carrying plasmas and often associated with significant anomalous collisionality [19–21]. Through a series of numerical experiments, the authors then argued that the collision frequency that arises from the IAT is sufficiently large to explain the anomalous resistivity that occurs in hollow cathode plumes.

In spite of the success the authors found in using the IAT collisionality to capture a number of experimentally observed trends, Mikellides *et al.* noted that the incorporation of this effect into their models was based on conjecture: There was no experimental confirmation of the IAT. To be sure, acoustic modes have been proposed to explain some of the salient trends in the observed frequency spectra of probes inserted into hollow cathode plumes [22,23], but the acoustic nature of these waves has never been directly measured. This lack of experimental confirmation brings a number of questions to mind about the role of the IAT in the operation of hollow cathodes: Does the IAT even exist in the plasma plume, and if so, how does it depend on operating conditions? Does it result in anomalous collision frequency? If yes, is the magnitude of the collisionality sufficient to justify the use of anomalous resistivity in the models?

The goal of this paper is to examine these questions experimentally and analytically. In the first section, we briefly review the theory of current-driven turbulence in an unmagnetized plasma. In the second section, we describe the experimental setup we employed to probe for the presence of acoustic turbulence and its effects in the plume of a 100-A LaB_6 hollow cathode. In the third section, we present the results of the experimental investigation and interpret them in the context of both turbulent theory and previously reported simulations of the cathode [24]. In the fourth and final section, we discuss the implications of IAT for hollow cathode performance and future modeling efforts.

*benjamin.a.jorns@jpl.nasa.gov

II. ION ACOUSTIC TURBULENCE THEORY

The ion acoustic instability is an electrostatic mode that naturally arises in plasmas where there is a large disparity in ion and electron temperatures $T_e/T_i \gg 1$ and where there is a significant electron drift velocity V_e. As such, the hollow cathode plume with its strong electron current and low ion temperature is a prime environment for the onset of this wave. In this section, we review the dispersion relation for the acoustic mode, and we explore the impact the instability can have on steady-state plasma parameters.

A. Dispersion relation

Since the collisionless processes that lead to the growth of the ion acoustic mode are inherently kinetic, we examine its dispersion relation through this formalism. Implicit in the following derivation is that the plasma is uniform as compared to the wavelength $\lambda \ll L$ where L denotes the characteristic gradient length and that the wave vector k is in the same direction as the electron drift V_e. While this second assumption can be violated for large amplitude waves (c.f. Refs. [19] and [25]) where loss processes lead to a saturation of modes in the parallel direction, we assume saturation is sufficiently weak at the onset of the instability that propagation is primarily in the direction of the electron drift. With this in mind, allowing for weak collisionality, the dispersion relation for acoustic modes is given by [26]

$$k^2\varepsilon(\omega,k) = 0 = k^2 - \frac{1}{2}\sum_{s=e,i}\frac{1}{\lambda_{ds}^2}\frac{Z_0'(\zeta^s)}{1+i(\nu_s/(k v_s\sqrt{2}))Z_0(\zeta^s)}, \tag{1}$$

where ε denotes the dielectric tensor, $\lambda_{ds} = (\epsilon_0 T_s/q^2 n_s)^{1/2}$ is the Debye length of the s species, and $Z_0(\zeta^s)$ is the plasma dispersion function:

$$Z_0(\zeta^s) = i\sqrt{\pi}e^{-(\zeta^s)^2}[1+\mathrm{erf}(i\zeta^s)] \tag{2}$$

$$\zeta^s = \frac{\omega + i\nu_s - kV_s}{k}\left(\frac{m_s}{2T_s}\right)^{1/2}. \tag{3}$$

Here ω is the wave frequency, k is the component of the wave vector parallel to the electron drift velocity, V_s is the drift speed of the s species in the parallel direction, v_s is the thermal speed, T_s is the temperature in units of energy, m_s is the species mass, $n_e = n_i = n_0$ is the background plasma density, and ν_s denotes the collision frequency.

We consider the following ordering that is characteristic of the ion acoustic mode as well as the cathode plasma $v_i \ll c_s \ll V_e \ll v_e$, where $c_s = \sqrt{T_e/m_i}$ is the ion sound speed. In this limit, it is only necessary to consider the cases where $|\zeta^e| \ll 1$ and $|\zeta^i| \gg 1$. This allows us to simplify Eq. (1),

$$k^2\varepsilon = 0 = k^2 - \omega_{pi}^2\left[-\frac{m_i}{T_e} + \frac{3T_i}{m_i}\frac{k^4}{(\omega')^4} + \frac{k^2}{(\omega')^2}\right] - i\left[-\frac{\omega'/k - V_e'}{\lambda_{de}^2 v_e}\left(\left(\frac{\pi}{2}\right)^{1/2} + \left(\frac{\pi}{2}-1\right)\frac{\nu_e}{k v_e}\right)\right.$$
$$\left. - \omega_{pi}^2\left(\frac{\nu_i}{\omega'}\left(\frac{k}{\omega'}\right)^2 + \left(\frac{\pi}{2}\right)^{1/2}\left(\frac{m_i}{T_i}\right)^{3/2}\frac{\omega'}{k}e^{-m_i(\omega'/k)^2/(2T_i)}\right)\right], \tag{4}$$

where $\omega_{pi} = \sqrt{q^2 n_0/\varepsilon_0 m_i}$ and we have transformed to the ion rest frame, $\omega' = \omega - kV_i$; $V_e' = V_e - V_i$. The solution of this equation for the frequency as a function of the wave number yields the dispersion of the acoustic mode. Finding this exact relationship is difficult in light of the equation's nonlinearity. Instead, we approximate the frequency dependence (c.f. Ref. [27], Chapter 4) by separating the dielectric tensor into its real and imaginary components: $\varepsilon(\omega,k) = \varepsilon_r + i\varepsilon_i$. Then, letting k be real, allowing $\omega = \omega_r + \omega_i i$, and assuming a small growth rate, $\omega_i \ll \omega_r$, we can Taylor expand the dielectric function with respect to ω_r. This yields two relations:

$$0 = \varepsilon_r(\omega_r,k), \quad \omega_i = -\frac{\varepsilon_i(\omega_r,k)}{\partial\varepsilon_r(\omega_r)/\partial\omega}.$$

Applying the first of these approximations to Eq. (4), we find

$$(\omega_r')^2 = k^2 c_s^2\left(\frac{1}{(\lambda_{de}k)^2+1} + 3\frac{T_i}{T_e}\right). \tag{5}$$

This is the kinetic dispersion for the real frequency of the ion acoustic mode. In the limit of cold ions $T_i \ll T_e$ and large wavelengths $k\lambda_{de} \ll 1$, we can see that this mode propagates with the ion sound speed $v_\phi = \omega/k = c_s$, whence it derives its name. Recalling that $\omega' = \omega - kV_i$, we can express the dispersion in the laboratory frame:

$$\omega \approx k[c_s + V_i], \tag{6}$$

where we have, for simplicity, made the substitution $\omega_r \to \omega$. Subject to the parameters typical for high-current cathodes, Eq. (6) is the experimental relationship between frequency and wave number we would expect to see if ion acoustic modes are present in the plasma.

We can determine the necessary conditions for these ion acoustic waves to appear by examining the imaginary part of the wave frequency. To this end, we use Eq. (4) and our Taylor expansion of the dielectric function to find

$$\omega_i = \frac{1}{2}c_s k\left[\left(\frac{V_e' - c_s}{v_e}\right)\left[\left(\frac{\pi}{2}\right)^{1/2} + \left(\frac{\pi}{2}-1\right)\frac{\nu_e}{k v_e}\right]\right.$$
$$\left. - \left(\frac{\pi}{2}\right)^{1/2}\left(\frac{T_e}{T_e}\right)^{3/2}e^{-T_e/2T_i}\right] - \frac{1}{2}\nu_i, \tag{7}$$

where we have made the simplification $\omega'/k \approx c_s$ in order to arrive at this compact form. In this expression, the first term stems from electron Landau damping, the second is from electron collisional effects, the third term represents ion Landau damping, and the fourth term is from collisional damping due to ions. Following Ref. [26], we note that subject

to the conditions for the development of the ion acoustic mode, we have $(\nu_e/kv_e) \approx (\nu_e/\omega)(m_e/m_i)^{1/2} \ll 1$. We therefore can neglect the second term in the growth rate as compared to the role of electron Landau damping. Similarly, assuming $T_e \gg T_i$, which is valid for the cathode plasma, we can neglect ion Landau damping compared to the ion collisional term. Equation (7) thus can be simplified to

$$\gamma = 2\omega_i = \omega' \left[\left(\frac{\pi}{2}\right)^{1/2} \left(\frac{V_e'}{v_e}\right) - \frac{\nu_i}{\omega'} \right], \tag{8}$$

where we have assumed $c_s \ll v_e$ and written the expression in terms of γ, the growth rate of the instability. Equation (8) embodies the dominant effects that can impact the formation of ion acoustic turbulence: growth due to inverse electron Landau damping and dissipation due to ion collisions. Since the electron Mach number can be very high $V_e' \gg v_e$ for the cathode plasma [24], it is reasonable to expect that the ion acoustic instability will exist in the plume.

B. Anomalous collision frequency

As we have seen from Eq. (8), the main driver for positive growth of the IAT is inverse electron Landau damping. This suggests that the energy for the ion acoustic instability comes at the expense of electron velocity. Effectively, the electrons are slowed down to add energy to the propagating waves. This energy transfer is irreversible and consequently can be modeled by an anomalous collision frequency. Weak-turbulent theory yields an expression for this frequency [25]:

$$\nu_{AN} \approx \omega_{pe} \frac{W}{n_0 T_e}. \tag{9}$$

Here ω_{pe} denotes the electron plasma frequency and W is the total energy density in the IAT given by

$$W = \frac{\varepsilon_0}{2} \frac{1}{V_k} \int \omega' [k\phi(k)]^2 \frac{\partial \epsilon_r}{\partial \omega'} d\mathbf{k}, \tag{10}$$

where the integral is over all of $\mathbf{k}$ space. We thus find the intuitive result from Eq. (9) that the larger the instability, the more energy it must extract from the electrons in order to be maintained.

It is possible to relate Eq. (9) to experimentally measurable quantities under the assumption that the wave vector is confined to a small cone centered around the direction of electron drift. Coupled with the relations $\omega' \approx kc_s$ and Eq. (4), this assumption allows us to proximate the volumetric integral by an integral in one dimension:

$$\nu_{AN} = \frac{\omega_{pe}}{T_e^2} \frac{1}{L_k} \int_0^{1/\lambda_{de}} [q\phi(k)]^2 dk, \tag{11}$$

where L_k is a characteristic length in k space and we have implemented an upper bound on the integral at the wave cutoff. Finally, we can convert to a frequency integral to find

$$\begin{aligned} \nu_{AN} &= \frac{\omega_{pe}}{T_e^2} \frac{1}{L_\omega} \int_0^{\omega_{pi}} [q\phi(\omega)]^2 d\omega \\ &= \frac{\omega_{pe}}{T_e^2} \sum_{\omega}^{\omega_{pi}} [q\phi(\omega)]^2, \end{aligned} \tag{12}$$

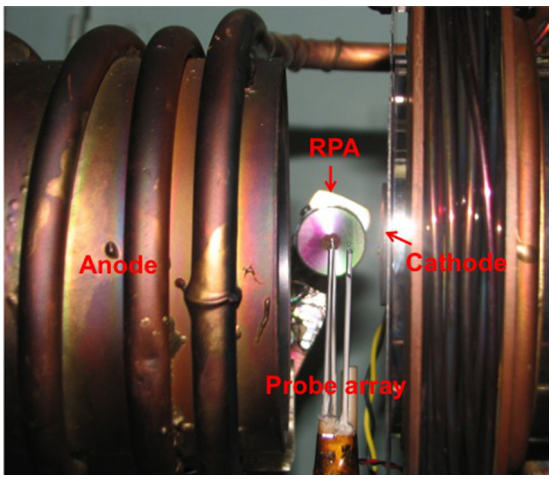

FIG. 1. (Color online) Photo of the 100-A hollow cathode experimental setup. A retarding potential analyzer (not used in this investigation) and the ion saturation probe array are also indicated.

where L_ω is a characteristic length in frequency space and we have written in the second line the integral as a sum over components in the frequency spectrum. Equation (12) is an estimate for the IAT anomalous collision frequency expressed in terms of the plasma density, electron temperature, and potential amplitude spectrum of the turbulence. This result is valid provided the IAT does in fact propagate in the cathode plume.

III. EXPERIMENTAL SETUP

In this section, we describe the cathode we investigated as well as the diagnostics we employed to detect the presence and impact of ion acoustic turbulence in the plume.

A. Cathode assembly

The 100-A cathode assembly (Fig. 1) in our experiment was designed with the purpose of achieving high current output. As reported in detail in Ref. [28], it consists of a graphite tube that houses a LaB_6 insert. A tungsten endplate with an orifice that is 12% the diameter of the cathode tube caps the end. The cathode tube is wrapped with a tantalum coaxial heater that in turn is housed in a graphite keeper. The ratio of the keeper orifice to the keeper diameter is 15%.

The setup was installed in the JPL High Current Test Facility, a 2.8 m × 1.3 m cylindrical chamber with vacuum maintained by two cryopumps. The base pressure of this facility was $\sim 10^{-7}$ T, and at the max flow condition we examined, 20 sccm xenon, the background pressure was maintained at 3.7×10^{-4} T. The anode consisted of a water-cooled, copper cylinder that was lined with tungsten and located ~3 cm downstream of the keeper face. The cathode assembly was surrounded by a solenoid capable of generating a magnetic field, although for the measurements reported here, there was no applied magnetic field.

B. Diagnostics

We performed two types of measurements during these trials in order to characterize the background plasma parameters and fluctuations. We discuss in the following the diagnostics we employed to make these measurements and the analysis techniques we used.

1. Langmuir probe

The background plasma density and temperature were measured with a single Langmuir probe located 0.75 cm downstream of the keeper face and placed on axis. The exposed element was 2 mm in length with a diameter of 0.51 mm. The reported electron temperature was inferred from an exponential fit to the probe IV trace (c.f. Ref. [29]), while we employed the thin sheath approximation for cylindrical probes to estimate density, $n_i = i_{\rm sat}/(0.61 q A_p \sqrt{T_e/m_i})$ where A_p denotes the probe area. The measurements reported here were generated from an average of 32 probe traces.

2. Ion saturation probes

To characterize the on-axis, current-driven fluctuations in the cathode plume, we employed the dual ion saturation probe setup shown in Fig. 1. It consisted of two exposed tungsten tips oriented along the axial direction. The length of each tip was 2 mm and each probe was biased to −30 V with a battery. The purpose of this diagnostic was to measure fluctuations in ion saturation current $i_{\rm sat}$ since these in turn serve as a proxy for plasma potential. In particular, for electrostatic modes such as the ion acoustic wave, we have

$$\phi \approx \frac{T_e}{q}\frac{\tilde{n}}{n_0}, \tag{13}$$

where $\tilde{n}$ denotes the fluctuations in the plasma density. The ion saturation current, however, is a direct proxy for density $i_{\rm sat} = \alpha n_i$ where α is a constant dependent on electron temperature and probe dimensions. Assuming electron temperature fluctuations are small compared to density perturbations then, we can see from Eq. (13) that

$$\phi \approx \frac{T_e}{q}\frac{\tilde{i}_{\rm sat}}{\bar{i}_{\rm sat}}, \tag{14}$$

where $\bar{i}_{\rm sat}$ denotes the time averaged quantity. By measuring the fluctuations in ion saturation current, we thus are able to infer fluctuations in potential.

Armed with this relation, we can characterize the nature of waves in the plasma by correlating the signal between probe tips. The principle of this technique can be illustrated by representing the fluctuations in the plasma with an eikonal approximation:

$$\phi = \sum_{\omega} \phi(\omega) e^{i(k(\omega)x - \omega t)}, \tag{15}$$

where $k(\omega)$ is the wave number at frequency ω and $\phi(\omega)$ denotes the complex amplitude of the wave with frequency ω. The fluctuation in potential as measured at two different positions in x is thus given by

$$\phi_1(t) = \sum_{\omega} \phi_1(\omega) e^{i(k(\omega)x_1 - \omega t)}, \tag{16}$$

$$\phi_2(t) = \sum_{\omega} \phi_2(\omega) e^{i(k(\omega)x_2 - \omega t)}. \tag{17}$$

By taking the Fourier transform $\mathcal{F}$ with respect to time of these two signals, we can find the following relation:

$$k(\omega) = \frac{1}{\Delta x}\tan^{-1}\left[\frac{\mathrm{Im}(\mathcal{F}[\phi_2(t)]\mathcal{F}^*[\phi_1(t)])}{\mathrm{Re}(\mathcal{F}[\phi_2(t)]\mathcal{F}^*[\phi_1(t)])}\right], \tag{18}$$

where $\Delta x = x_2 - x_1$. This expression provides a means to measure the wave number $k(\omega)$ along the vector between the two probe tips (axial in our case) where the range of discernible wave numbers is dictated by the separation between probes, $|k| < \pi/\Delta x$.

The accuracy of this approach can be improved in a noisy environment by averaging over a number of time signals. However, if there are multiple modes present in the plasma, i.e., multiple wave numbers for a fixed frequency, this technique can be errant. In order to resolve the distribution of k at a fixed ω, we employ the histogram technique first proposed by Beall [30]. In particular, we perform a number M of time samples and evaluate the wave number as a function of frequency for each run according to Eq. (18). We then bin the k values and weight them according to

$$S(\omega,k) = \frac{1}{M}\sum_{j=1}^{M} I_{0,\Delta k}[k - k^j(\omega)]\frac{1}{2}\left[P_1^{(j)}(\omega) + P_2^{(j)}(\omega)\right]. \tag{19}$$

Here j indicates the run number, $P_1^{(j)}, P_2^{(j)}$, are the power spectra of the two signals, and we have defined the function,

$$I_{0,\Delta k}(x) = \begin{cases} 1 & |x| < \Delta k \\ 0 & |x| > \Delta k \end{cases},$$

where Δk is the width of the bin. Equation (19) provides a means for us to visualize the dominant frequencies and wave numbers in $k-\omega$ space. In particular, the results for wave detection that we report in the following section were generated from Eq. (19) and are represented as intensity plots in $k-\omega$ with a wave number resolution of $\Delta k = 0.84\ \mathrm{m}^{-1}$ (for 150 bins) and a frequency resolution of $\Delta f = 10$ kHz.

IV. RESULTS

In the following section, we present the results of a parametric investigation of the oscillations in the plume of the 100-A LaB_6 cathode. All measurements were performed on axis at 0.75 cm from the keeper face. We examined operating conditions at four flow rates of xenon, 8 sccm, 10 sccm, 15 sccm, and 20 sccm over the discharge current range $I_D = 20$ A − 130 A.

A. Background measurements

We show measurements in Fig. 2 of the electron temperature and density as a function of the cathode operating condition. From the plot on the bottom, we find the physically intuitive result that the density increases monotonically with discharge current at all flow conditions. Similarly, from the plot on the top, we immediately can see that the overall magnitude of electron temperature decreases with flow rate. This latter trend is consistent with previous experimental investigations [28] and suggests that collisional damping leads to an overall depression in electron temperature.

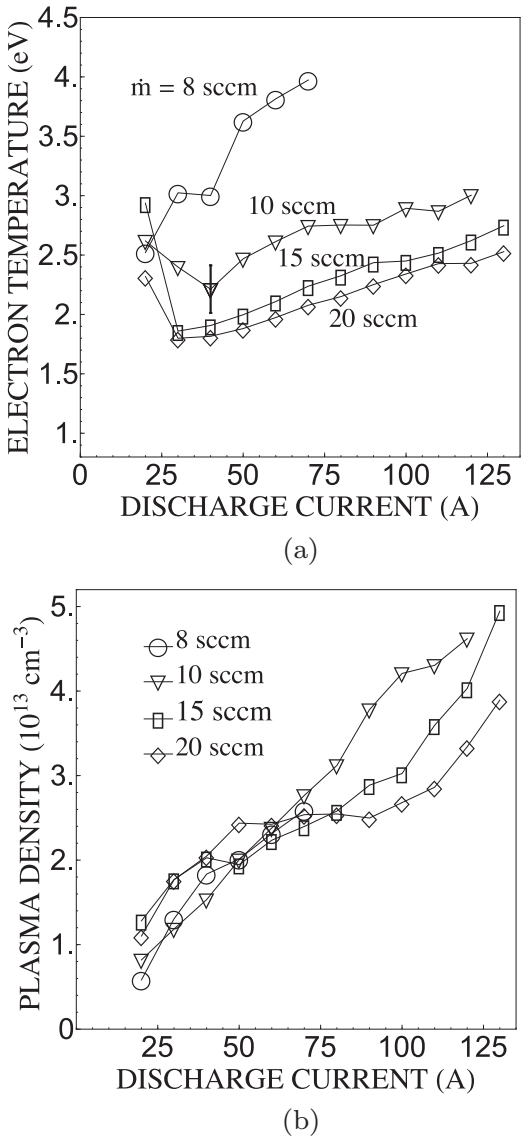

FIG. 2. (a) Electron temperature (b) and plasma density as functions of discharge current at four different flow rates. A representative error bar is shown for the temperature while the density is accurate to within 50%.

The trends for temperature as a function of discharge current are not as easily explained. In particular, at 8 sccm we can see the temperature strictly increases with discharge current, while at higher flow rates the electron temperature is nonmonotonic—passing through a minimum value and then rising. This is in direct contrast to the results reported in Ref. [28] where it was found that *inside* the same cathode tube and at fixed flow rate, the electron temperature decreased monotonically with discharge current. This discrepancy between internal and external measurements may stem from the relationship between electron temperature and resistive heating in the plume. In particular, although the electron temperature falls inside the cathode with increasing discharge current due to internal processes, at sufficiently high discharge currents, local effects in the plume—such as the onset of the IAT—may give rise to enhanced collisionality. This in turn could lead to local heating and a subsequent increase in electron temperature. The initial decrease in temperature with current we observe in Fig. 2 thus could reflect the fact that at small discharge current, the resistive heating in the plume is sufficiently low that the plume temperature is a proxy for the internal cathode processes (decreasing temperature with current). It is only when the resistive effects in the plasma become sufficiently high that the external resistivity becomes dominant and the temperature in the plume deviates from the experimentally observed trends inside the cathode. This is a possibility we explore in the following sections.

B. Turbulence measurements

In order to examine the nature of the fluctuations in the cathode plume, we employed the methods and techniques we outlined in Sec. III to generate the Beall intensity plots shown in Fig. 3. These figures serve to illustrate the frequency and axial wave number character of the fluctuations in the cathode plume as a function of increasing discharge current at fixed flow rate (10 sccm).

Most notably, we can see that while at $I_D = 30$ A the intensity plot is dominated by low frequency (<100 kHz) and dispersionless content, a high frequency mode with a linear dispersion begins to emerge at increasing discharge current. This is clearly illustrated by the transition from $I_D = 60$ A to $I_D = 110$ A where in the former case the high frequency content is comparable in amplitude to the low frequency components and in the latter case the high frequency mode is dominant with a maximum near 800 kHz. The strong linearity from both plots that exhibit the high frequency mode allows us to identify the effects of aliasing. Since the probe spacing is a finite width Δx, modes with wavelength λ shorter than the spacing between the probe tips appear as lower wave numbers with $k = 2\pi(\lambda^{-1} - n/\Delta x)$ where $n = \lfloor \Delta x/\lambda \rfloor$. Given the periodicity of the dispersions in Fig. 3, however, we can adjust for the aliasing by translating the plot with respect to wave number. An example of this correction is shown in Fig. 4 and reflects the true dispersion of the mode.

The linear nature of the high frequency mode in the direction of electron drift strongly suggests that it is the ion acoustic instability ($\omega \propto k$). This conclusion is bolstered by measurements of the phase velocity exhibited by the mode, which we have made by fitting a line to the dispersion plot. An example of such a fit is illustrated by the dotted line in Fig. 4, and the results of these fits over the investigated parameter space is shown in Fig. 5. We note that the plotted points correspond to the conditions where we could observe the linear dispersion in the Beall plots, and the reason why the high flow rate case, $\dot{m} = 20$ sccm, is not shown is because we could not resolve the high frequency mode above the noise. For comparison, we also include in Fig. 5 a plot of the calculated sound speed $c_s = \sqrt{T_e/m_i}$ as a function of operating conditions. The correspondence between the measured phase velocity and the ion sound speed provides the strongest evidence yet that the observed linear mode is the ion acoustic instability. There is an offset in all cases of ~3 km/s such that the measured phase velocity does not correspond directly to the sound speed, but we note that this discrepancy can be explained by the fact that the phase velocity of the wave is the sum of the ion sound speed and the ion drift velocity

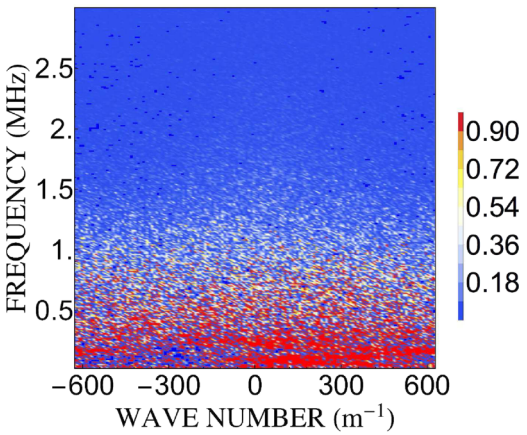

(a)

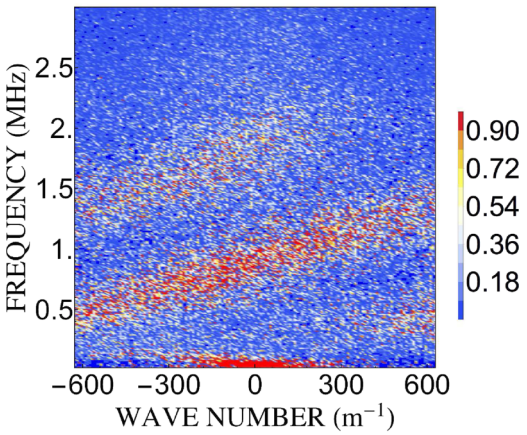

(b)

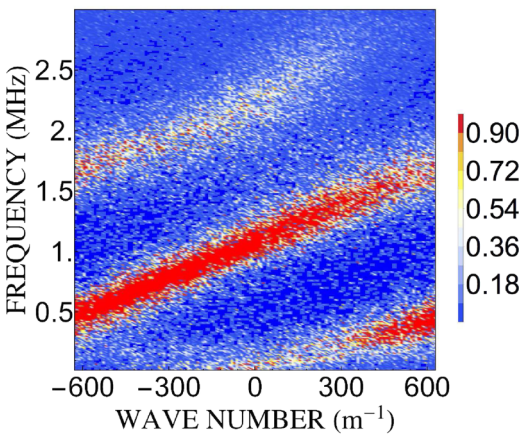

(c)

FIG. 3. (Color online) Beall plots with increasing current at the flow condition $\dot{m} = 10$ sccm: (a) $I_D = 30$ A; (b) $I_D = 60$ A; and (c) $I_D = 110$ A. Each plot is normalized to its maximum and has a frequency resolution of 10 kHz.

[Eq. (6)]. This would indicate an axial ion drift of ∼3 km/s, which is consistent with previous laser induced fluorescence measurements of ion velocities in a hollow cathode [31] as well as simulations of our 100-A LaB_6 high current cathode [24]. With this result, we have for the first time experimental evidence that ion acoustic turbulence exists in the cathode

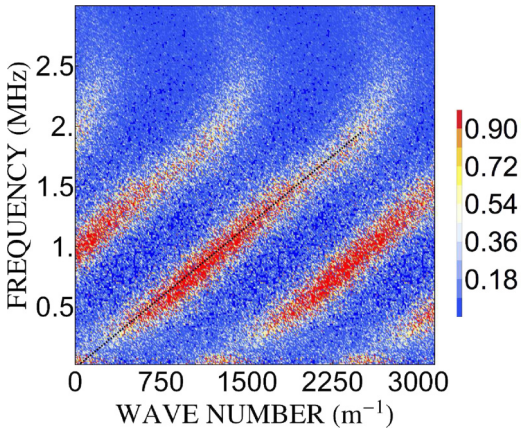

FIG. 4. (Color online) Beall intensity plot where aliasing is corrected for the case of $I_D = 90$ A and $\dot{m} = 10$ sccm. The dotted line is a best fit to the linear dispersion of the acoustic mode.

plume. This corroborates the assumptions about the local plasma we made in Sec. II as well as the findings of previous modeling efforts that showed the conditions were right for this mode to onset [1,16,24].

We show in Fig. 6 the frequency dependence of the power in the IAT as a function of discharge current. The low frequency peak at $f = 50$–100 kHz corresponds to the dispersionless mode identified in Fig. 3 and is likely associated with the coherent ionization instability previously discussed by Goebel *et al.* [15]. On the other hand, at frequency values above this range, we can see that for the unambiguous cases where the IAT exists ($I_D > 60$ A as demonstrated by Fig. 3) each power spectrum has a characteristic shape, exhibiting a maximum in the range 400–1000 kHz and decreasing with frequency at lower and higher values. The cutoff of the IAT amplitude at low frequency can be attributed to ion-neutral damping—the growth rate changes sign when the wave frequency drops below the ion neutral collision frequency [Eq. (8)]. The decrease in amplitude at high frequency, on the other hand, cannot be explained by the linear growth rate since this term indicates the IAT amplitude should be larger with increasing frequency. This departure from linear theory may be the result of nonlinear saturation effects such as electron trapping [32], ion resonance broadening [33,34], and nonlinear Landau damping [35,36]. All of these processes serve to transfer energy from higher frequency modes to lower ones with the consequence that the IAT spectrum exhibits an inverse dependence on frequency at high values, $\phi^2 \propto \omega^\eta$ where $\eta < 0$. In support of this conclusion, we show in Fig. 7(a) a sample log-log plot of the power spectrum of the IAT where we have fit a line to the drop-off in the spectrum that occurs after the peak. The slope of this line is -2.8, which corresponds to a decrease in power spectrum amplitude of $\omega^{-2.8}$. We similarly have examined the decay of the power spectra for all of the flow rate conditions and discharge current values where we could identify from the Beall plot technique that the ion acoustic mode was present. The slopes we found from this parametric investigation are shown in Fig. 7(b) and range from $\eta = -2$ to -4. For comparison, we plot the theoretically predicted exponents for saturation due to electron trapping, $\eta = -2.4$ [32], and ion resonance broadening, $\eta = -2.6$ [34]. The close correspondence

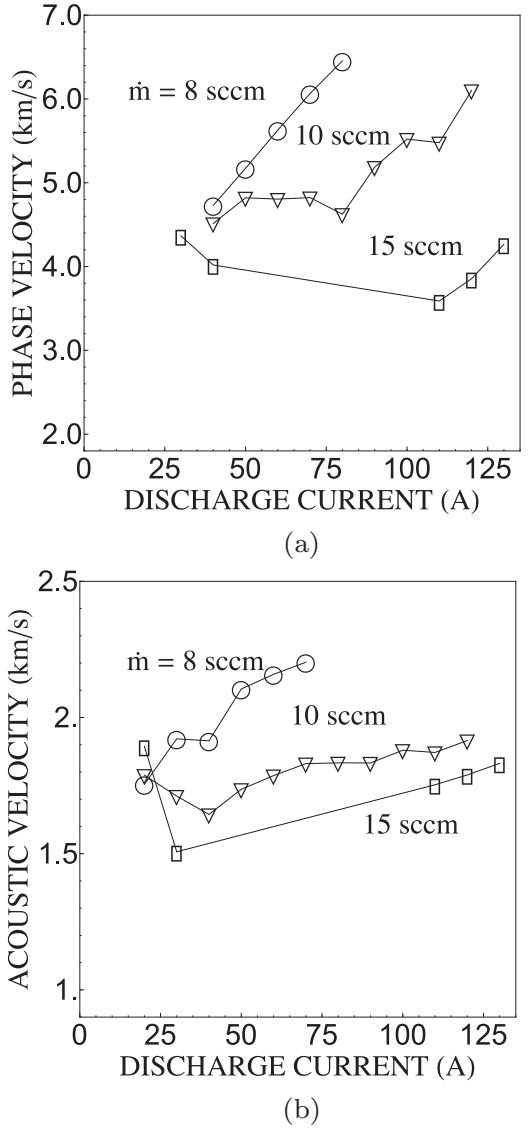

FIG. 5. (a) Phase velocity of the acoustic mode as a function of discharge current at different mass flow rates. The IAT could not be resolved at $\dot{m} = 20$ sccm, and the absence of points in the $\dot{m} = 15$ sccm reflects our inability to detect the dispersion of the mode for these current values. (b) The calculated sound speed c_s at the same conditions.

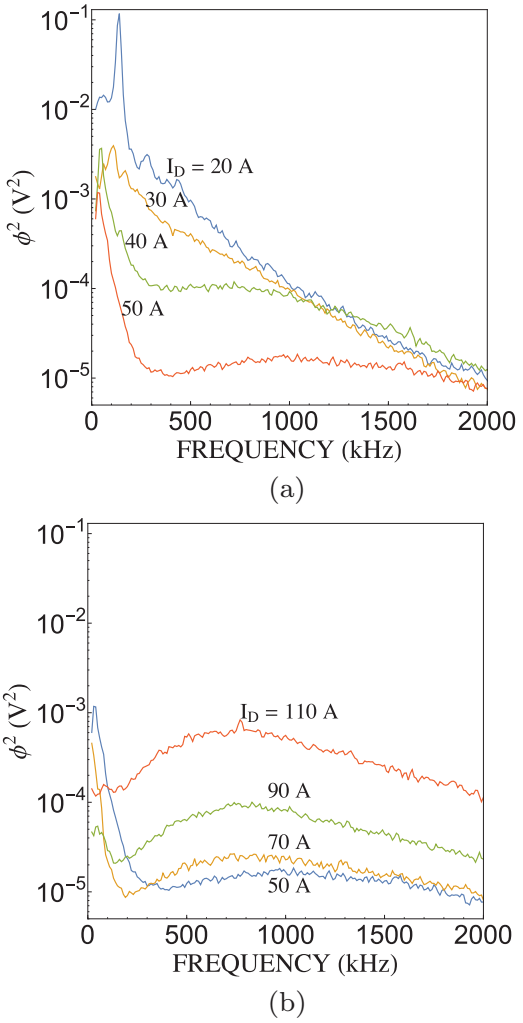

FIG. 6. (Color online) Power spectra for $\dot{m} = 10$ sccm as a function of increasing current. The top figure (a) illustrates the initial emergence of the IAT while the bottom plot (b) shows the growth of IAT with increasing current.

between these predictions and the measured slopes suggests the associated saturation processes may in part be responsible for the observed spectra. Nonlinear ion Landau damping, on the other hand, appears to be less of a significant contributor given its theoretically predicted exponent, $\eta = -1$ [35], is outside the measured values. Regardless of the mechanism driving the shape of the turbulent spectra, however, we can use the characteristic decrease with frequency as a supplementary metric for the presence of the IAT in the cathode plume. In particular, even though the low frequency, nonpropagating ionization oscillations make it difficult to distinguish the IAT from the Beall plots at low current conditions, e.g., $I_D = 30 - 40$ A, the characteristic decrease with frequency exhibited by these power spectra suggests that the IAT is still present.

Keeping this metric in mind, we can see from Fig. 6 that the amplitude of the IAT has a nonmonotonic dependence on discharge current, exhibiting a minimum at $I_D = 50$ A. The reason for this trend is not immediately clear but may be the result of changing electron drift influencing the growth rate [Eq. (8)] or the dependence of nonlinear effects on discharge current that are not included in our formulation. These effects could include the aforementioned saturation processes such as ion resonance broadening and electron trapping, or it is possible there could be other effects at play such as nonlinear interactions of the acoustic waves with other modes concurrently excited in the plasma. Mendonca and Bingham [37], for example, demonstrated that high frequency electron turbulence can alter the effective dispersion relation of ion acoustic waves. While fully examining these nonlinear effects is beyond the scope of this investigation, we note that determining the dependence of each of these nonlinear effects on discharge current ultimately may shed light on the nonmonotonic trend with current exhibited by the IAT. With that said, it may not be necessary to invoke nonlinear

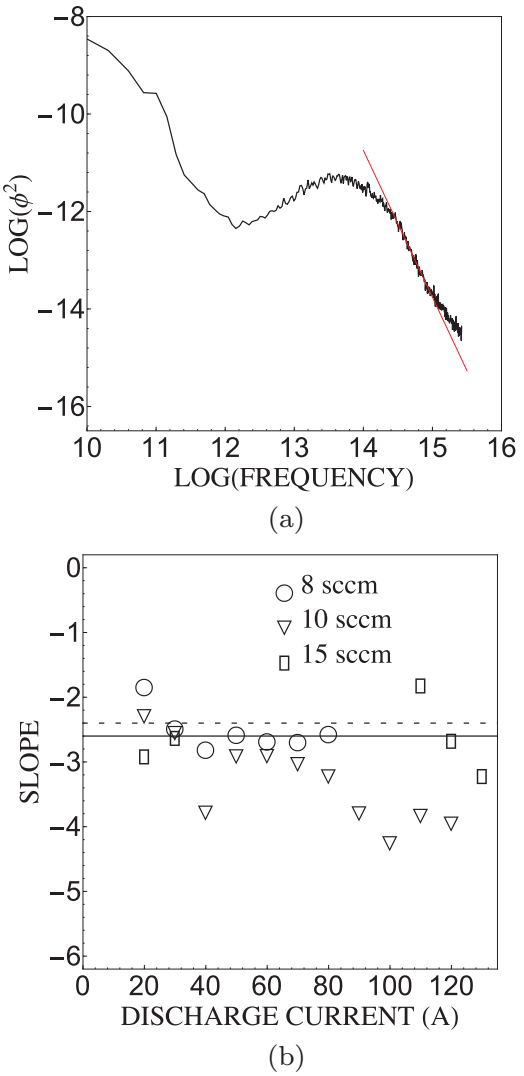

FIG. 7. (Color online) (a) Natural log-log plot of the measured power spectrum at $I_D = 100$ A and $\dot{m} = 10$ sccm. The red line is a best fit to the decay of the spectrum. (b) The slopes of the best fits to the linear decay of the turbulent spectra as a function of discharge current for three different flow rates. The dotted line with value -2.4 corresponds to the electron trapping theory for the saturated turbulent spectrum while the solid line at -2.6 represents the ion-resonance broadening theory for saturation.

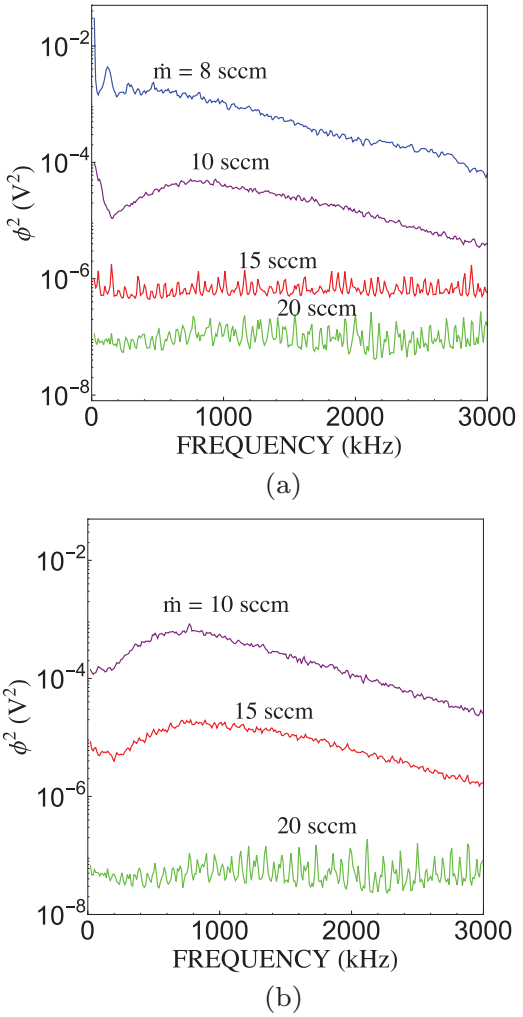

FIG. 8. (Color online) Semilog plots of power spectra for fixed currents and different flow rates: (a) $I_D = 80$ A and (b) $I_D = 110$ A.

processes to explain the dependence of the IAT amplitude on flow rate. From the cases illustrated in Fig. 8, it is evident that at fixed discharge current the amplitude of the power spectrum monotonically decreases with flow rate. Since neutral density increases with flow rate, this result suggests that enhanced ion-neutral collisionality could result in the observed damping of the spectrum.

Given the dependence of Eq. (12) on the turbulent amplitude, we expect that the anomalous collision frequency will exhibit similar dependence on flow rate and current as that demonstrated by the IAT. In the next section, we use our steady-state plasma parameters and our measurement of the frequency dependence of the power spectra to determine these trends.

C. Anomalous collision frequency

We show in Fig. 9(a) the anomalous collision frequency of the IAT calculated from our measurements of the power spectra and Eq. (12). It is apparent from this plot that for the cases where we can resolve the IAT, the collision frequency exhibits the same trends as the ones we outlined for the power spectrum amplitude in the previous section. The collision frequency depends nonmonotonically on discharge current but ultimately increases with discharge current at high values. Similarly, at high flow rates, the collision frequency decreases. This correspondence is an unsurprising result given that Eq. (12) depends on the amplitude of the power spectrum. In this same vein, since electron resistivity is a function of collision frequency, we can relate the trends we see in Fig. 9(a) to the electron temperature results we discussed in Sec. IV A. In particular, we pointed out that the growth of the anomalous collision frequency in the cathode plume may explain the increase in electron temperature with the discharge current depicted in Fig. 2. The same trends exhibited by the anomalous collisionality and electron temperature support this thesis.

In order to illustrate the relative importance of the anomalous collision frequency compared to the classical effects that

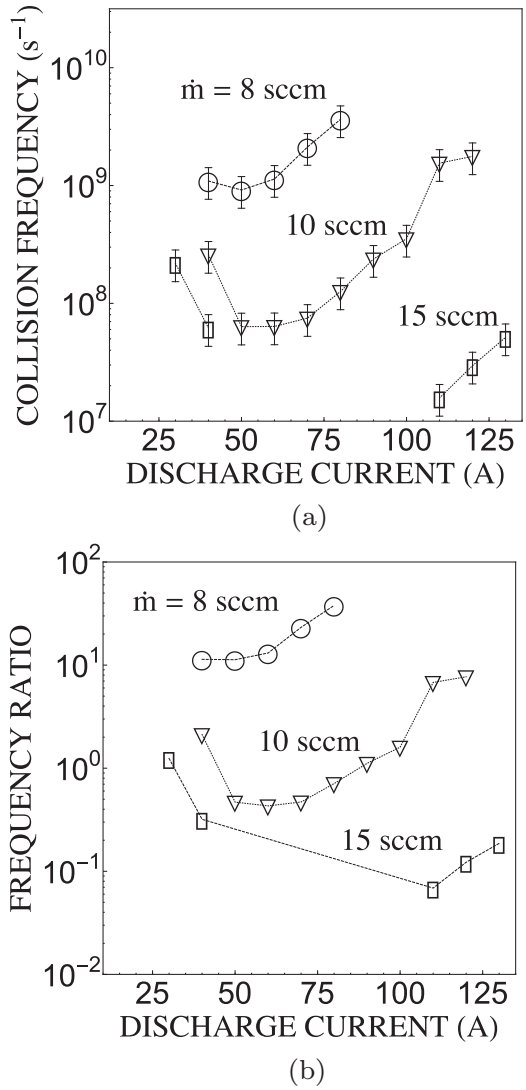

FIG. 9. (a) Anomalous collision frequency due to the IAT. (b) Ratio of anomalous collision frequency to classical electron-ion collision frequency based on measurements of the electron temperature and density. Maximum error is ±30%.

occur in our cathode plasma, we show in Fig. 9(b) the ratio of ν_{AN} to the calculated electron-ion collision frequency:

$$\nu_{ei} = 2.9 \times 10^{-12} n_0 T_e^{-3/2} \left[23 - 0.5 \log \left(\frac{10^{-6} n_0}{T_e^3} \right) \right], \quad (20)$$

where n_0 is the background density in units of m^{-3}. From this plot we can see that there are a number of operating conditions—most notably high current to flow ratios—where the anomalous collision term is dominant. This is the first experimental evidence that not only are there nonclassical effects in the plume but these effects can be larger (under the right operating conditions) than classical terms. In turn, this result directly supports the conclusions from previous attempts to model the cathode plasma [1,16,24] where it was found that the steady-state parameters of the cathode plume cannot be explained by ordinary interspecies collisions.

V. DISCUSSION

We can summarize the results from our theoretical and experimental work concerning the contribution of the IAT to the anomalous collision frequency with the following observations.

(1) The IAT exists in the hollow cathode plume.

(2) The IAT power spectrum is characterized by a maximum value of 400–1000 kHz and exhibits an inverse dependence on frequency at high frequency values.

(3) The IAT amplitude at first decreases and then increases with discharge current at fixed flow rate. It decreases with flow rate at fixed discharge current.

(4) The experimentally measured anomalous collision frequency exceeds classical frequencies for a number of operating conditions—most notably at high current to flow ratios.

These observations have a direct impact on our understanding of the underlying physical processes in the hollow cathode plume. In particular, there are a number of operating conditions where the anomalous collision frequency from the IAT cannot be ignored. Rather, this effect must be taken into consideration if we want to successfully model the plasma parameters such as potential, electron temperature, and density in the cathode plume. Creating models capable of such high fidelity is essential both for efforts to determine long-term cathode behavior as well as attempts to realize new designs. These capabilities will become increasingly important as the next generation of electric propulsion missions calls for cathodes with higher discharge currents.

VI. CONCLUSION

In this work, we have presented a parametric investigation of ion acoustic turbulence in the plume of a 100-A LaB_6 cathode. We have reviewed the theory for how IAT can lead to the onset of anomalous collisions at the expense of the electron drift in the hollow cathode discharge, and through a series of probe-based investigations, we have implemented an experimental setup in which we were able to detect successfully the onset and growth of the IAT at high discharge current. We furthermore have investigated the details of the power spectra exhibited by these waves over a wide range of discharge current and flow rate. Our findings suggest the following mechanism for IAT onset: While the IAT is driven unstable by electron drift, nonlinear processes lead to a redistribution of the wave energy from high frequencies to low values while ion collisional damping leads to cutoff of the wave at low frequencies.

Through direct measurement, we have confirmed that the anomalous collisionality from the IAT is dominant over classical processes over a wide range of operating conditions. By identifying the IAT as a main contributor to the collisionality in the hollow cathode plume, we thus have helped shed light on a dominant, nonclassical process that is fundamental to the operation of high current cathodes. The new insights and increased confidence in model fidelity that stem from this work will become increasingly important as the need for higher current cathodes becomes more pressing.

ACKNOWLEDGMENTS

The research described in this paper was carried out by the Jet Propulsion Laboratory, California Institute of Technology, under a contract with the National Aeronautics and Space Administration and funded through the internal Research and Technology Development program.

[1] I. G. Mikellides, I. Katz, D. M. Goebel, and K. K. Jameson, J. Appl. Phys. **101**, 063301 (2007).
[2] J. Polk *et al.*, *An Overview of the Results from an 8200 Hour Wear Test of the NSTAR Ion Thruster* (AIAA Paper 99-2446, AIAA, Reston, 1999).
[3] A. Sengupta, J. R. Brophy, and K. D. Goodfellow, *Status of the Extended Life Test of the Deep Space 1 Flight Spare Ion Engine after 30, 352 Hours of Operation* (AIAA Paper 03-4558, AIAA, Reston, 2003).
[4] M. D. Rayman, in *IAF Abstracts, 34th COSPAR Scientific Assembly* (2nd World Space Congress, Houston, TX, 2002).
[5] C. Koppel, F. Marchandise, M. Prioul, D. Estublier, and F. Darnon, in *41st Joint Propulsion Conference and Exhibit, Tucson, AZ, 10–13 July 2005* (AIAA Report 2005-3671, Reston, 2005).
[6] C. Garner, J. Brophy, S. Mikes, and M. Rayman, in *44th AIAA/ASME/SAE/ASEE Joint Propulsion Conference, 20–23 July, 2008, Hartford, CT* (AIAA Report 2008-4917, Reston, 2008).
[7] J. R. Brophy, J. E. Polk, T. M. Randolph, and J. W. Dankanich, in *44th Joint Propulsion Conference, Hartford, CT, 2008* (AIAA Report 2008-5184, Reston, 2008).
[8] J. Brophy and C. Garner, in *AIAA/ASME/SAE/ASEE 24th Joint Propulsion Conference, Boston, MA* (AIAA Paper 88-2193, Reston, 1988).
[9] V. Friedly and P. Wilbur, J. Propul. Power **8**, 635 (2008).
[10] I. Kameyama, *Effects of Neutral Density on Energetic Ions Produced Near High-Current Hollow Cathodes* (Technical Report NASA CR-204154, Washington, DC, 1997).
[11] G. Williams, M. T. Domonkos, and J. M. Chavez, in *27th International Electric Propulsion Conference, Pasadena, CA* (IEPC-01-310, Electric Rocket Propulsion Society, Fairview Park, 2001), pp. 15–19.
[12] I. Katz, I. G. Mikellides, D. M. Goebel, K. K. Jameson, and L. Johnson, in *42nd AIAA/ASME/SAE/ASEE Joint Propulsion Conference and Exhibit, Sacramento, CA, 2006* (AIAA Report 2006-4485, Reston, 2006).
[13] J. E. Foster and M. J. Patterson, J. Propul. Power **21**, 144 (2005).
[14] A. Gallimore and J. Rovey, J. Propul. Power **23**, 1271 (2007).
[15] D. M. Goebel, K. K. Jameson, I. Katz, and I. G. Mikellides, Phys. Plasmas **14**, 103508 (2007).
[16] I. G. Mikellides, I. Katz, D. M. Goebel, K. K. Jameson, and J. E. Polk, J. Propul. Power **24**, 866 (2008).
[17] E. Chu, D. M. Goebel, and R. E. Wirz, J. Propul. Power **29**, 1155 (2013).
[18] I. G. Mikellides, I. Katz, D. M. Goebel, and J. E. Polk, J. Appl. Phys. **98**, 113303 (2005).
[19] V. Bychenkov, V. Silin, and S. Uryupin, Physics Reports **164**, 119 (1988).
[20] H. de Kluiver, N. Perepelkin, and A. Hirose, Physics Reports **199**, 281 (1991).
[21] W. Horton, *Turbulent Transport in Magnetized Plasmas* (World Scientific, Singapore, 2012).
[22] D. Fitzgerald, Ph.D thesis, Colorado State University, 1983.
[23] C. C. Farnell, J. D. Williams, and C. C. Farnell, Plasma Sources Sci. Technol. **20**, 025006 (2011).
[24] I. G. Mikellides, D. M. Goebel, B. A. Jorns, J. Polk, and P. Guerrero, in *33rd International Electric Propulsion Conference, The George Washington University, Washington, D. C. October 6–10, 2013* (IEPC 2007-124, Electric Rocket Propulsion Society, Fairview Park, 2013).
[25] R. Sagdeev and A. Galeev, *Nonlinear Plasma Theory*, *Frontiers in Physics* (W. A. Benjamin, New York,1969).
[26] D. B. Fenneman, M. Raether, and M. Yamada, Phys. Fluids **16**, 871 (1973).
[27] T. Stix, *Waves in Plasmas* (AIP, New York, 1992).
[28] E. Chu and D. M. Goebel, Plasma Science, IEEE Transactions on **40**, 2133 (2012).
[29] F. F. Chen, Langmuir, in *Mini-Course on Plasma Diagnostics, IEEE-ICOPS Meeting, Jeju, Korea*, 2003 (IEEE, Piscataway, 2003).
[30] J. M. Beall, Y. C. Kim, and E. J. Powers, J. Appl. Phys. **53**, 3933 (1982).
[31] J. Williams, T. Smith, M. Domonkos, A. Gallimore, and R. Drake, IEEE Transactions on Plasma Science **28**, 1664 (2000).
[32] K. Nishikawa and C.-S. Wu, Phys. Rev. Lett. **23**, 1020 (1969).
[33] A. M. Sleeper, J. Weinstock, and B. Bezzerides, Phys. Fluids **16**, 1508 (1973).
[34] A. Basu, A. S. Sharma, and A. C. Das, Plasma Phys. Controlled Fusion **27**, 433 (1985).
[35] B. Kadomtsev, *Plasma Turbulence* (Academic Press, Waltham, 1965).
[36] D.-I. Choi and J. Wendell Horton, Phys. Fluids **17**, 2048 (1974).
[37] J. T. Mendonca and R. Bingham, Physics of Plasmas **9**, 2604 (2002).